

## Numerical simulation of wind loading on roadside noise mitigation structures

K.T. TSE<sup>1</sup>, Yi Yang<sup>\*1,2</sup>, K.M. Shum<sup>3</sup> and Zhuangning Xie<sup>2</sup>

<sup>1</sup>Department of Civil and Environmental Engineering, The Hong Kong University of Science and Technology, Clear Water Bay, Kowloon, Hong Kong

<sup>2</sup>State Key Laboratory of Sub-tropical Building Science, South China University of Technology, Guangzhou 580641, China

<sup>3</sup>The CLP Power Wind/Wave Tunnel Facility, The Hong Kong University of Science and Technology, Clear Water Bay, Kowloon, Hong Kong

(Received April 26, 2012, Revised December 27, 2012, Accepted February 28, 2013)

**Abstract.** Numerical research on four typical configurations of noise mitigation structures and their characteristics of wind loads are reported in this paper. The turbulence model as well the model parameters, the modeling of the equilibrium atmospheric boundary layer, the mesh discretization etc., were carefully considered in the numerical model to improve the numerical accuracy. Also a numerical validation of one configuration with the wind tunnel test data was made. Through detailed analyses of the wind load characteristics with the inclined part and the wind incidence angle, it was found that the addition of an inclined part to a noise mitigation structure at-grade would affect the mean net pressure coefficients on the vertical part, and that the extent of this effect depends on the length of the inclined part itself. The magnitudes of the mean net pressure coefficients for both the vertical part and the inclined part of noise mitigation structure at-grade tended to increase with length of inclined part. Finally, a comparison with the wind load code British/European Standard BS EN 1991-1-4:2005 was made and the envelope of the mean net pressure coefficients of the noise mitigation structures was given for design purposes. The current research should be helpful to improve current wind codes by providing more reasonable wind pressure coefficients for different configurations of noise mitigation structures.

**Keywords:** wind loads; noise mitigation structure; SST  $k-\epsilon$  turbulence model; equilibrium atmospheric boundary layer

### 1. Introduction

The rapid development of infrastructure has raised public concern about vehicular noise generated on highways, and other major roads, that are often located in close proximity to residential estates and public areas. Noise mitigation structures (NMS), or noise barriers are generally built along the roadsides, forming a useful tool to protect residential estates, and public areas in close proximity, from the unfavorable vehicular noise pollution. A noise mitigation structure is a light-weight wind sensitive structure; however, there are currently no specific

---

\*Corresponding author, Professor, E-mail: [ctyangyi@scut.edu.cn](mailto:ctyangyi@scut.edu.cn)

provisions in design codes and/or standards in some regions and countries, such as Hong Kong and mainland China, for the appropriate assessment of wind forces acting on NMS.

Some wind tunnel test studies of NMS have already been carried out. For example, two sets of wind tunnel test results on free-standing vertical walls were reported by Letchford and Holmes (1994). The wind tunnel tests were conducted using a model length scale of 1:75 with simulated wind flow above open terrain. They found that large wind loads were generated at the windward end of a wall for an angle of incidence of  $45^\circ$  and that those loads increased markedly with increasing wall length. The results were incorporated into design data in the 1989 version of the Australian Standard for Wind Loads and ESDU data sheets. Letchford and Robertson (1999), using pressure measurements, and Letchford (2001), using a simple one component force balance, conducted a number of further parametric wind tunnel studies for single vertical walls, to quantify the effects of aspect ratio, clearance ratio, wind direction, porosity and return walls at the end of the main wall. Baker (2001) analyzed the unsteady wind loading data on a 18 m long and 2 m high wall using standard statistical techniques as well as the proper orthogonal decomposition and wavelet analysis. Different characteristics of the fluctuating wind pressure on both the front face and the rear face were analyzed.

Holmes (2001) reported a series of wind-tunnel test study of boundary-layer wind loads on parallel noise barriers of approximately 20 representative situations on freeways and motorways. The details of the experimental techniques and the main results of the study as well as the comparison with previous wind-tunnel tests were given. More recently, Geurts and van Bentum (2010) conducted wind tunnel measurements on T-shaped free standing walls and inclined free-standing walls. The results for free-standing walls with T-tops showed that the net pressure coefficient of the vertical part of the wall may decrease due to the application of a T-top. Shum *et al.* (2011) performed wind tunnel tests on several NMS both at-grade and on bridge with/without inclined parts. Zheng and Wang (2009) researched the wind load shape coefficients of NMS, both on-ground and on bridges, by combining CFD simulation, wind pressure measurement tests and wind force measurements. They suggested the wind load shape coefficients of 1.65 for NMS on bridges and 1.99 for NMS on ground respectively. This contradicts the results of Holmes (2001) discussed above. Numerical simulation of the wind loads on NMS on bridge were discussed by Wang *et al.* (2011) mainly focussing on the effect of induced wind loads by running cars. It concluded that such induced wind loads should be considered for the structure anti-fatigue design.

Although there have been significant developments in the determination of wind loads for NMS, the results are mostly limited to simple vertical walls. NMS in practice, for instance in Hong Kong and major Chinese cities, have shapes and forms that are not explicitly covered by local or international standards and codes or in the research literature. To accurately quantify the wind loading on the NMS, a series of numerical simulations has been carried out for four types of NMS at-grade situations, and the results are compared in terms of barrier shape and wind incidence angle. Finally, the envelopes of the mean net pressure coefficients from all the computed angles of attack are presented and the average mean net pressure coefficients over the designated pressure zones are compared with those provided in BS EN 1991-1-4:2005.

## 2. Model configurations

Fig. 1 shows vertical noise mitigation structure and vertical noise mitigation structure with an inclined upper part, which are typically used in Hong Kong. Although wind-induced pressures on vertical walls were treated in detail by Letchford and Holmes (1994) and Holmes (2001), there was no information for wind-induced pressures on vertical walls with an inclined upper part. Therefore, numerical simulations of wind loadings on these two NMS configurations were conducted.



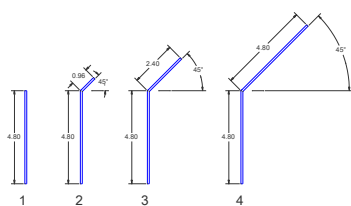
Vertical noise NMS at-grade  
(after Shum *et al.* 2011)



Vertical NMS with an inclined part at-grade  
(after Shum *et al.* 2011)

Fig. 1 Typical noise mitigation structures in Hong Kong

A vertical noise mitigation structure with an inclined upper part with an inclination angle of 45° was selected for the research, as this geometry is the most commonly-used configuration in Hong Kong. Three types varying the lengths of the inclined upper part are chosen here, and Fig. 2 shows the prototype scale dimensions of the total four NMS configurations. The ratio of the length to the height is set as L/H=30.



Configuration No.	H (m)	I (m)	$\alpha$ (deg)
Type 1	4.8	-	-
Type 2	4.8	0.96	45
Type 3	4.8	2.4	45
Type 4	4.8	4.8	45

Fig. 2 Noise mitigation structure configurations

### 3. Numerical model

#### 3.1 Turbulence model

The SST  $k$ - $\omega$  model, which was developed by Menter (1994) is adopted here to model the turbulent flow. It takes into account of the transport of the turbulent shear stress and gives highly accurate predictions of the onset and the amount of flow separation under adverse pressure gradients (Menter 1994). Its applicability of blunt body flow was validated through the comparison between the numerical results and the wind tunnel test data of a low-rise building (Yang *et al.* 2008).

The SST  $k$ - $\omega$  model combines the robust and accurate formulation of the  $k$ - $\omega$  model in the near-wall region with the free-stream independence of the  $k$ - $\varepsilon$  model in the far field. A blending function,  $F_1$ , is adopted to bridge them. The equations of the Wilcox  $k$ - $\omega$  model being multiplied by function  $F_1$ , and the transformed  $k$ - $\varepsilon$  equations by a function  $1-F_1$ , form the corresponding turbulent kinetic energy (TKE) ( $k$ ) equation and the turbulent frequency ( $\omega$ ) equation of the SST model as follows

$$\frac{\partial \rho k}{\partial t} + \frac{\partial}{\partial x_j} \left( \rho u_j k - \left( \mu + \frac{\mu_t}{\sigma_k} \right) \frac{\partial k}{\partial x_j} \right) = P_k - C_\mu \rho \omega k \quad (1)$$

$$\frac{\partial \rho \omega}{\partial t} + \frac{\partial}{\partial x_j} \left( \rho u_j \omega - \left( \mu + \frac{\mu_t}{\sigma_\omega} \right) \frac{\partial \omega}{\partial x_j} \right) = \alpha \frac{\omega}{k} P_k - \beta \rho \omega^2 + 2(1-F_1) \frac{\rho}{\sigma_{\omega 2} \omega} \frac{\partial k}{\partial x_j} \frac{\partial \omega}{\partial x_j} \quad (2)$$

The coefficients of the new model are a linear combination of the corresponding coefficients of the underlying models

$$\phi = F_1 \phi_1 + (1-F_1) \phi_2 \quad (3)$$

where  $F_1$  and  $F_2$  are two blending functions,  $\phi = \{\alpha, \beta, \sigma_k, \sigma_\omega\}$ .

The numerical result of blunt body flow was heavily influenced by the turbulence parameters, which was concluded by the authors through detailed comparisons (Yang *et al.* 2008). Therefore, here the parameters were taken as the ‘‘SST2 model’’ system as follows proposed in Yang *et al.* (2008) to improve the numerical accuracy. The non-dimensional turbulence parameter  $C_\mu$  in the model is the ratio of the square friction velocity to the turbulence kinetic energy, which was taken as 0.04, and the new values of the parameters of the inner layer Wilcox  $k$ - $\omega$  model were given as  $\alpha_1 = 0.413$ ,  $\beta_1 = 0.0333$ ,  $\sigma_{k1} = 1.176$  and  $\sigma_{\omega1} = 2$ , and those of the outer layer  $k$ - $\varepsilon$  model were given as  $\alpha_2 = 0.02$ ,  $\beta_2 = 0.0368$ ,  $\sigma_{k2} = 1.0$  and  $\sigma_{\omega2} = 1.168$ . This set of turbulence parameters had been proved to be applicable for blunt body flow and could obtain relatively better results through the research of a low-rise building (Yang *et al.* 2008).

#### 3.2 Boundary conditions

Modeling an equilibrium atmospheric boundary layer is an important pre-condition for numerical simulation of flows around buildings. The horizontal inhomogeneity of the simulated atmospheric boundary layer (ABL) will result in additional errors to numerical results and sometimes they are significant, which was emphasized by many researchers (Richards and Quinn 2002, Franke 2007, Blocken *et al.* 2007).

The problem of constructing an equilibrium boundary layer was further investigated by the authors from the viewpoint of the turbulence model itself (Yang *et al.* 2009). The solution to the TKE equation of the standard  $k$ - $\varepsilon$  model were derived firstly based on the assumption of the local equilibrium of turbulence, and then a new set of inflow turbulence boundary conditions for modeling equilibrium atmosphere boundary layer was proposed (Yang *et al.* 2009). The capability of these inflow boundary conditions producing an equilibrium ABL in the standard  $k$ - $\varepsilon$  model has been numerically verified and demonstrated.

Recently, the performance and applicability of this new set of inflow boundary condition model was validated (Gorlé *et al.* 2010, O'Sullivan *et al.* 2011). Moreover, the proposed new idea as well as the boundary condition model have been adopted in the numerical simulations of ABL flow and related transport phenomena by many researchers (Barić *et al.* 2010, Kozmar 2011, Labovský and Jelemenský 2011, Parente *et al.* 2011).

This method was newly extended to the SST  $k$ - $\omega$  model, and its ability of generating the equilibrium atmospheric ABL has been numerically validated (Yang *et al.* 2012). Here we adopt the proposed inflow turbulence boundary conditions as follows

$$k = \frac{u_*^2}{\sqrt{C_\mu}} \sqrt{C_1 \cdot \ln\left(\frac{z+z_0}{z_0}\right) + C_2} \quad (4)$$

$$\varepsilon = \frac{u_*^3}{\kappa(z+z_0)} \sqrt{C_1 \ln\left(\frac{z+z_0}{z_0}\right) + C_2} \quad (5)$$

$$\omega = \frac{u_*}{\kappa\sqrt{C_\mu}} \frac{1}{z+z_0} \quad (6)$$

where  $C_1$  and  $C_2$  are two adjustable parameters independent on the frictional velocity  $u_*$  and the roughness length  $z_0$ . Normally, they could be determined by nonlinear fitting of experimental data of TKE. Therefore, they become the characteristic parameters reflecting the turbulence level of inflow.

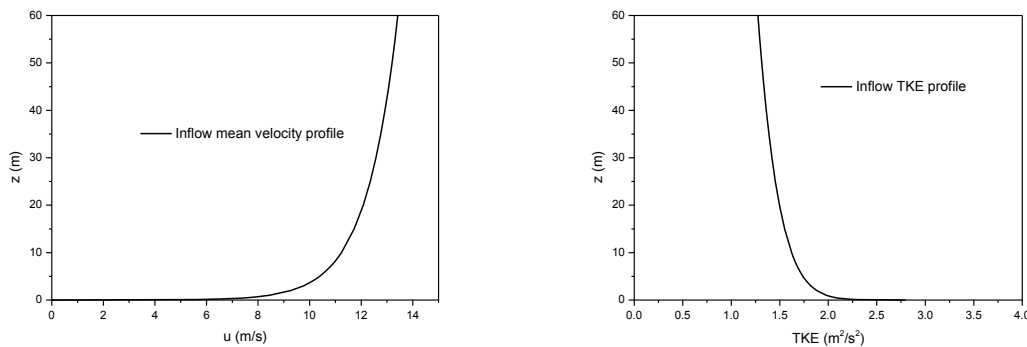


Fig. 3 Mean velocity and TKE profiles of simulated boundary layer

A boundary-layer wind model corresponding to wind flowing above deep open water, as

specified in the Code of Practice of Wind Effects in Hong Kong (Buildings Department 2004), was simulated using equations summarized in Table 1, in which every boundary surfaces of the basic numerical model and their corresponding boundary conditions are given. The frictional velocity of the inflow mean velocity profile  $u$  is set as  $u_* = 0.4 \text{ m/s}$ , the roughness length is  $z_0 = 0.001 \text{ m}$ , and the two constants are  $C_1 = -0.36$  and  $C_2 = 5.0$  respectively. Although the mean velocity profile  $u$  in Table 1, which was expressed by the logarithmic law, was different from the HK Wind Code of the power law, the profiles of those two different descriptions of the wind velocity characteristics defined by the parameters in Table 1 are very close. The inflow mean velocity and TKE profiles are shown as Fig. 3.

The outflow boundary is modeled as the fully developed outflow, which means the gradients of all physical quantities are zero. The two side boundaries and the top boundary, on the other hand, could be reasonably defined as the free slip surface, which means both the normal velocity components and the gradients of all other physical quantities should be zero.

The ground boundary is modeled as the rough wall, and the modified wall function considering roughness,  $u_p / u_* = \ln\{u_p^* / [v(1+0.3k_s^+)]\} / k + 5.2$ , is employed. Blocken *et al.* (2007) derived relations between the equivalent sand-grain roughness height for the ABL,  $K_{s,ABL}$ , and the roughness length  $z_0$ ,  $K_{s,ABL} \approx 30z_0$ .

The surfaces of the noise mitigation structure are modeled as “thin” walls with zero thickness as listed in Table 1.

Table 1 Boundary conditions of the basic numerical model

Location		Boundary conditions
	Defining the mean velocity	$u = (u_* / \kappa) \times \ln[(z + z_0) / z_0], \quad v = 0, \quad w = 0;$
Inflow face	( $u$ ), TKE( $k$ ) and turbulence frequency( $\omega$ )	$k = (u_*^2 / \sqrt{C_\mu}) \sqrt{C_1 \cdot \ln[(z + z_0) / z_0] + C_2},$ $\omega = u_* / (k \sqrt{C_\mu}) / (z + z_0)$
Outflow face	Fully developed outflow	$\frac{\partial}{\partial x}(u, v, w, k, \omega) = 0$
Side faces and top face	Free slip	$v = 0, \quad \frac{\partial}{\partial z}(u, w, k, \omega) = 0; \quad w = 0, \quad \frac{\partial}{\partial z}(u, v, k, \omega) = 0$
Surfaces of NMS	wall	$u = 0, \quad v = 0, \quad w = 0$
ground	wall	Wall function was employed and rough wall modification was introduced (Durbin and Petterson Reif, 2001). Roughness height $K_s = 0.03m$

### 3.3 Numerical parameters

The calculation domain was divided into two parts, inner domain containing the NMS and outer domain, and they are discretized by structured hexahedral mesh cells and unstructured hexahedral mesh cells respectively, as shown in Fig. 4. The boundary layer mesh cells were supplemented close to the NMS walls so as to improve the solution. The total number of mesh cells reached about 5,000,000. The minimum mesh size close to the building model was about  $y^+ \approx 30$ . Fig. 2 illustrates the face meshes of the numerical model for the Type 2 at the inflow attack angle of  $\theta = 0^\circ$ . The size of the computational domain was set as large as 600 m (W)  $\times$  60 m (H)  $\times$  1200 m (L) to satisfy both the requirements of the blockage ratio (less than 3%), and the domain length in the along wind direction (full scale model was built in the numerical model).

The flow was assumed to be incompressible and steady, and the SIMPLE algorithm was used for pressure-velocity coupling. The second order upwind difference scheme was adopted for all the convective terms in momentum equation and turbulence model equations. The diffusive terms were discretized by the second order central difference scheme. The flow field was initialized by the values set for the inlet boundary conditions. The convergence criteria of the scaled residuals for all the variables and the continuity equation were set as  $10^{-5}$ . The numerical simulation was carried out with the commercial CFD software of Ansys CFX 13 in the workstation of the CLP Power Wind/Wave Tunnel Facility at the Hong Kong University of Science and Technology, which is configured with 8-core CPU with 3.0 GHz and 16 G memory. It took about 18 hours for a typical case to reach convergence.

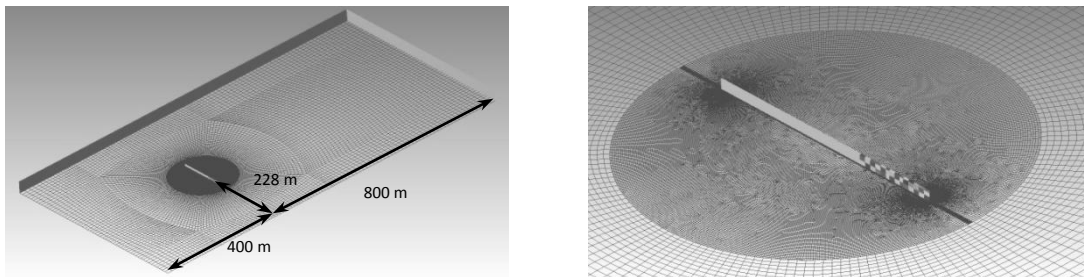


Fig. 4 Mesh arrangement of numerical model of Type 2 at wind attack angle of  $0^\circ$

## 4. Numerical simulation results and analyses

For each NMS type, four inflow attack angles,  $0^\circ$ ,  $45^\circ$ ,  $135^\circ$  and  $180^\circ$  were computed, therefore, there are totally 12 different conditions (For  $0^\circ$  attack angle, there are only 2 different cases for the property of symmetry) for result analysis and discussion.

First, we define the mean nett pressure coefficient  $C_{pn}$ , which was determined from the dimensionless mean wind pressure acting on the exposed faces of the NMS models as

$$C_{pn} = \frac{P_w(t) - P_l(t)}{0.5 \rho u_{h,ref}^2} \quad (7)$$

where  $P_w(t)$  and  $P_l(t)$  are the nett wind pressures force acting on the windward and leeward faces

of the models; the density of air,  $\rho$ , was taken as 1.225 kg/m<sup>3</sup>;  $\bar{u}_{h,ref}$  is the mean wind speed at a height,  $h_{ref}$ , equivalent to the top of the vertical part of the noise mitigation structure;  $A$  is the area of the panel. The wind incidence angle relative to the NMS is defined in Fig. 5 and the sign convention used to define the mean nett pressure coefficient acting on the inclined part is also given in Fig. 5.

In order to better describe the wind load distributions in space, the whole NMS wall faces were divided into several small panels starting from the ends. Only the portion of wall extending from the windward free end to a distance of approximate 10  $H$  was investigated, as it represents the most unfavorable part for wind load design. The dimensions of the panel were set as 0.5  $H$  or  $I$  (L)\*0.75  $H$  ( $H$ ), as shown in Fig. 6. Finally, a total of three lines (2 lines for Type 1) multiplying 14 panels each line were chosen to describe the characteristics of wind load distribution for NMS structures.

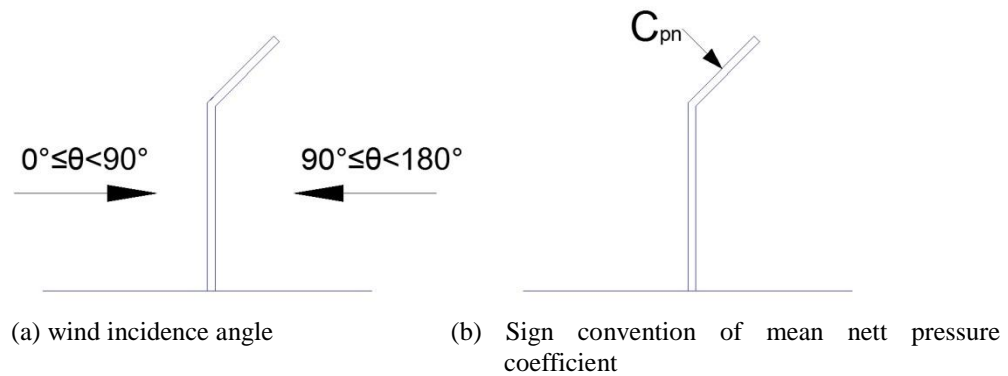


Fig. 5 Definitions of the wind incidence angle and the sign convention of mean nett pressure coefficient for the inclined part

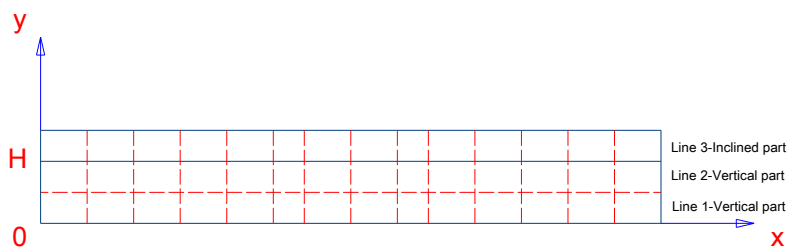


Fig. 6 The scheme of the panel partition of the NMS faces

#### 4.1 Numerical validation

Although the numerical model was built carefully to consider all important aspects, such as the turbulence model, the boundary conditions and the mesh discretization, a numerical validation was also carried out to confirm the reliability of the numerical results reported in this paper. One of the

wind tunnel tests of noise mitigation structures (Shum *et al.* 2011), similar to the Type 3, was used for this purpose .

Wind tunnel tests of different configurations of NMS both at-ground and on bridge were carried out in the high speed test section of the CLP Power Wind/Wave Tunnel Facility at the Hong Kong University of Science and Technology (Shum *et al.* 2011). A boundary-layer wind model corresponding to wind flowing above deep open water, as specified in the Code of Practice of Wind Effects in Hong Kong (Buildings Department 2004), was simulated using a combination of solid wooden fences and roughness elements over a 21 m fetch length. Mean wind speeds and turbulent intensities, measured at the location where the model was positioned, were within 5% of the target profiles. The wind tunnel models were fabricated at a length scale of 1:75 and the maximum blockage ratio was 5.3%. A photo of the wind tunnel test of a NMS model was shown in Fig. 7. The pressure-taps were installed on both surfaces of the model to allow the wind pressures to be measured simultaneously on both sides of the noise mitigation structures. Each pressure-tap was connected individually to one dedicated channel of a high speed pressure scanner that allowed surface pressures to be measured simultaneously on both faces of the NMS. The test data were sampled at 400 Hz for a duration of 169 seconds, equivalent to approximately 1 hour in prototype scale.



Fig. 7 Wind tunnel model of the noise mitigation structure at-grade (after Shum *et al.* 2011)

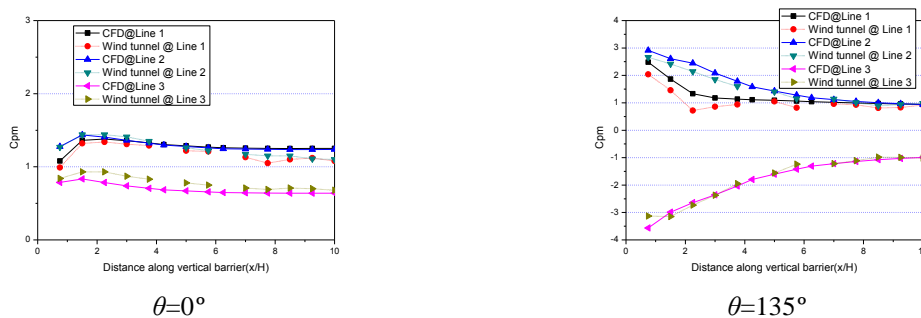


Fig. 8 Comparisons of the mean net pressure coefficients for Type 3 at  $\theta=0^\circ$  and  $\theta=135^\circ$

Fig. 8 shows the comparisons of the mean net pressure coefficients at two main wind attack angles,  $\theta=0^\circ$  and  $135^\circ$ , representing the vertical and typical oblique wind directions respectively.

From the figure, it can be seen clearly that the numerical results are very close to those of the wind tunnel test on the whole, although relatively obvious deviations along Line 1 at  $\theta=135^\circ$  occur, especially for the panels near the windward free end. It might be attributable to the relatively larger numerical errors near the free end close to the ground. In this area, the strong separated corner vortex in the leeward side originating from the free end was generated under the oblique wind flow, which had been illustrated in Fig. 14 for similar NWS Type 4. Correspondingly, a large negative pressure gradient on the leeward surface appeared. The finite difference scheme is insufficient to accurately reflect this rapid change of the wind pressure for the relative coarse mesh cells.

Despite of the discrepancies, it could be reasonably concluded that the numerical model is capable to provide relatively high accurate results, therefore, it can be employed for the systematic numerical research on the mean wind load characteristics of NMS.

#### 4.2 Effect of inclined part

Mean nett pressure coefficients on NMS for wind incident angle of  $0^\circ$  and  $180^\circ$  are plotted in Figs. 9-10. For these two wind directions, the wind is normal to the models, and the effects of the inclined part on the wind pressure distribution could be clearly illustrated.

It can be seen from Figs. 9-10 that the mean nett pressure coefficients for the vertical parts of configuration No.2 are very close to those of lowest inclined part of configuration No.1 for  $\theta=0^\circ$  and  $\theta=180^\circ$ , while the wind loads increase regularly with the length of inclined parts increasing. Some notable enhancements can be observed in the mean nett pressure coefficients for some vertical panels of configurations No.3 and No.4. Except the panels near the windward free end, the magnitudes of the mean nett pressure coefficients on both the vertical part and the inclined part of configuration No.4 are always larger than those of the other configurations, as shown in the figures.

This indicates that the addition of an inclined part affects the mean nett pressure coefficient on the lower vertical part, depending on its length. Fig.11 illustrates the mean nett pressure coefficient contours on the leeward surfaces of the lower vertical parts for 4 types of NMS configurations at  $\theta=0^\circ$ , clearly indicating this general trend, i.e., the absolute values of the negative wind pressure gradually increasing with the length of the inclined parts.

The magnitudes of the mean nett pressure coefficients on both the inclined part itself, and the lower vertical part, tend to increase with the inclined length ( $l$ ) when the wind is normal to the noise mitigation structure. The results also show that the largest wind load occurs on the second or third panel closely near the windward free end.

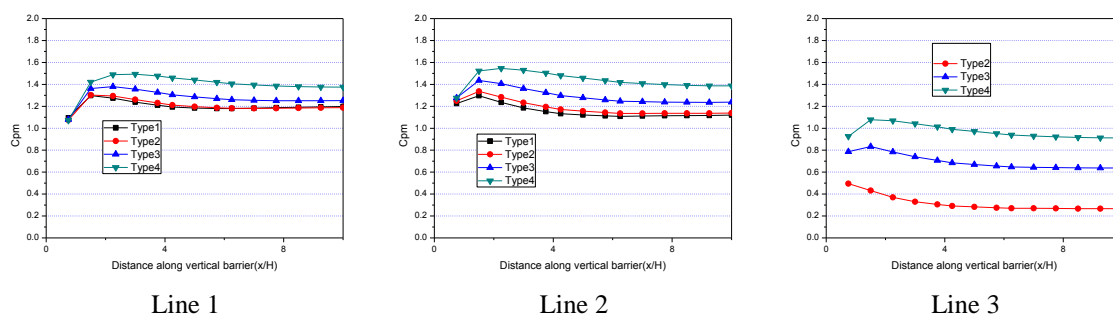


Fig. 9 Mean nett pressure coefficients for 4 types of NMS configurations at  $\theta=0^\circ$

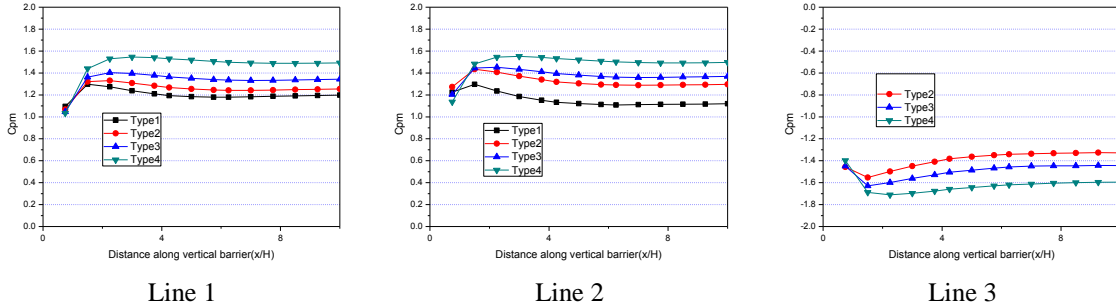


Fig. 10 Mean net pressure coefficients for 4 types of NMS configurations at  $\theta=180^\circ$

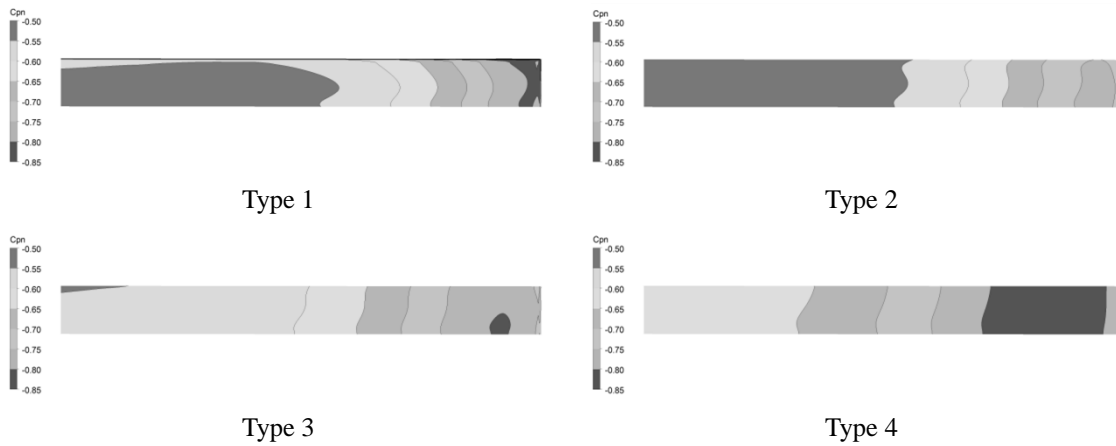


Fig. 11 Contours of the mean net pressure coefficients on the leeward surfaces for 4 types of NMS configurations at  $\theta=0$

### 4.3 Effect of wind incidence angle

Mean net pressure coefficients on NMS are plotted in Fig. 12 for all incident wind directions,  $\theta$ , of  $0^\circ$ ,  $45^\circ$ ,  $135^\circ$  and  $180^\circ$ . For  $\theta=45^\circ$  and  $135^\circ$  wind directions, the wind is oblique to the vertical part of the models.

It can be seen that the magnitudes of the mean net pressure coefficients on both the vertical and inclined parts of panels near the windward free end of all configurations, i.e., Type No.1-No.4, increase significantly for the incidence angles of  $45^\circ$  and  $135^\circ$ . It means the oblique wind results the strong corner vortex in the leeward side of the windward free end, and large negative wind pressure occurs, which is illustrated as Fig. 13 of Type No.4 at the incidence angle of  $135^\circ$

The mean net pressure coefficients near the middle of the wall of configurations No.3 and No.4 are generally slightly larger than those of configurations No.1 and No.2 for an incidence angle of  $45^\circ$  or  $135^\circ$ , tending to increase with the length of inclined part, which is due to the same observations revealed at the vertical incidence angle of  $0^\circ$  or  $180^\circ$  in the previous section.

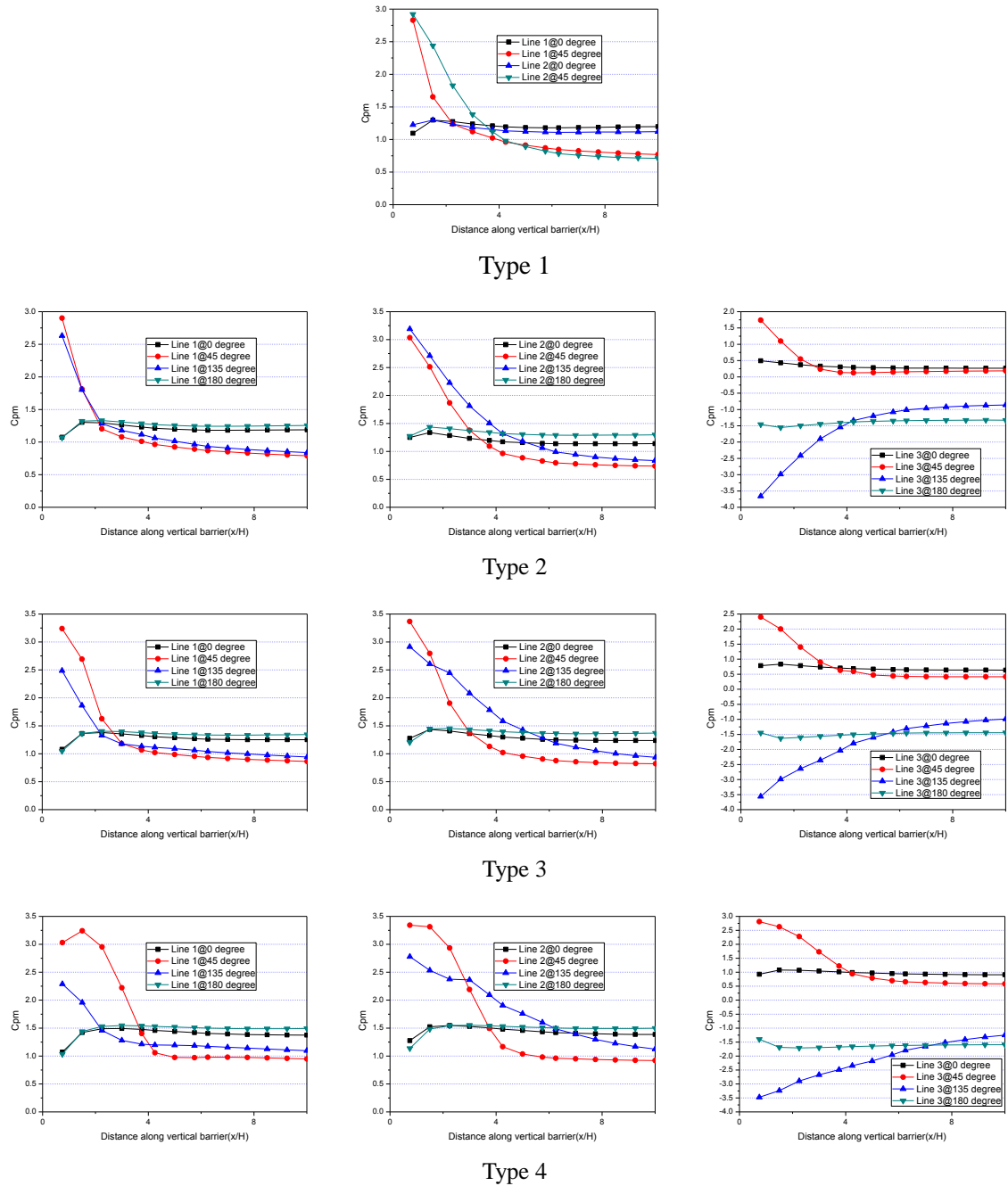


Fig. 12 Mean nett pressure coefficients for 4 types of NMS configurations at  $\theta=0^\circ, 45^\circ, 135^\circ$  and  $180^\circ$

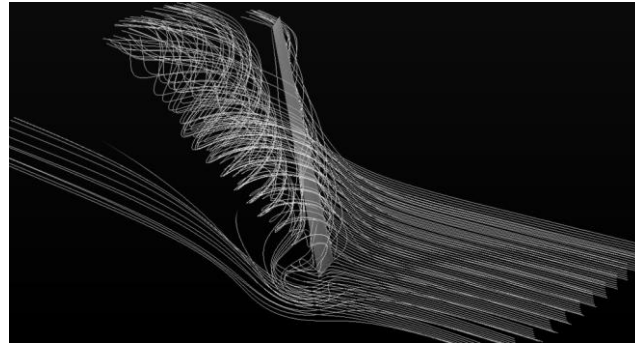


Fig. 13 Streamline of Type 4 at the incidence angle of 135°, which indicates the strong corner vortex in the leeward side of the NMS initiating from the wind free end arises

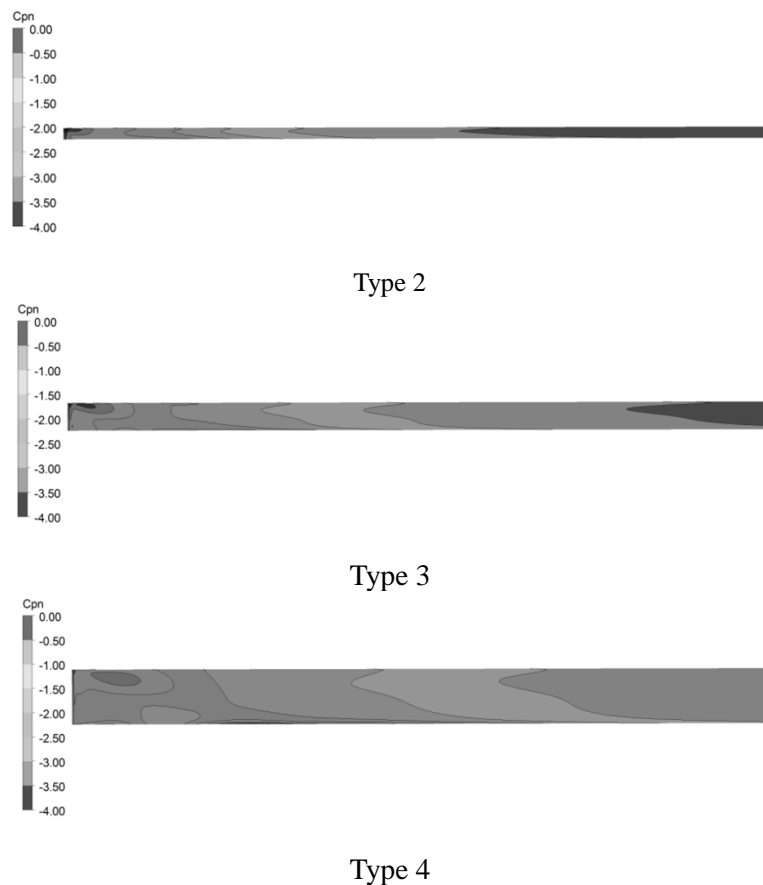


Fig. 14 Contours of the mean net pressure coefficients on the leeward surfaces for 3 types of NMS configurations with inclined parts at  $\theta=135^\circ$

For the oblique incidence angle of  $45^\circ$ , the magnitudes of the mean nett pressure coefficients on the inclined part of configuration No.4 are apparently larger than those of configurations No.2 and No.3. However, for the incidence angle of  $135^\circ$ , the magnitudes of the mean nett pressure coefficients on the inclined part of configuration No.4 are also slightly larger than those of configurations No.2 and No.3, except for the 1 panel near windward free end, which is shown in Fig. 14.

For all wind attack angles, among others, the oblique incidence angle of  $135^\circ$  is the most unfavorable wind direction for the inclined part, and this tendency gradually decreases and switch to  $45^\circ$  for the vertical part, with the heights of the panel reducing and the inclined part length (I) increasing.

#### 4.4 Envelope of mean nett pressure coefficients

Envelopes of mean nett pressure coefficients are presented in Fig. 15 to allow a thorough comparison for the different configurations of NMS. The envelope of mean nett pressure coefficients for the inclined part is the upper bound of the absolute mean nett pressure coefficients from different wind incidence angles. The corresponding average mean nett pressure coefficients over the designated zones A, B and C are tabulated in Tables 2-3.

It can be seen from Fig. 15 and Table 2 that the mean nett pressure coefficients over the vertical part of configurations No.2, No.3 and No.4 increased with the length of the inclined part. Table 2 also indicates that the pressure coefficient over zone A was underestimated by BS EN 1991-1-4:2005. For example, the average mean nett pressure coefficient for the vertical part of configuration No.4 in the area A ( $0 < X < 2H$ ) is about 3.33 suggested by the numerical results, while this value gets only 2.3 according to the code of BS EN 1991-1-4:2005, which is about 30% lower than the current result.

The magnitude of the mean nett pressure coefficients for the inclined part of NMS increases with the length of the inclined part, as shown in Fig.15. Table 3 indicates that the average mean nett pressure coefficients on zone A of the inclined part of configurations No.2, No.3 and No.4 are very similar, and the average mean nett pressure coefficients on the inclined part in zones B and C increase with increasing length (I).

Table 2 Average mean nett pressure coefficients for the vertical part of NMS at-grade

Zone	Configuration No.1	Configuration No.2	Configuration No.3	Configuration No.4	BS EN 1991-1-4:2005
A( $0 < X < 2H$ )	2.68	2.95	3.08	3.33	2.3*
B( $2H < X < 4H$ )	1.47	1.85	2.10	2.47	1.7
C( $X > 4H$ )	1.19	1.30	1.40	1.58	1.2

\*This value is the average pressure coefficient over the segment with a distance of 2H from the windward end

Wind loads are usually the dominant design load for the lightweight noise structures. Through

the detailed numerical simulations on four typical NMS, it is shown that the current wind load codes, for example, BS EN 1991-1-4:2005, still need further improvement of wind pressure coefficients for different configurations of noise mitigation structure. For example, the proposed average mean nett pressure coefficients for the vertical part could be appropriately raised, and the coefficients for the inclined part could be supplemented, considering the recent research and findings on those structures. Similar findings had been also reported by the wind tunnel test results of Geurts and van Bentum (2010) and (Shum *et al.* 2011). All this work is helpful in improving current wind codes and hence improve the wind-resistant safety of NMS structural designs.

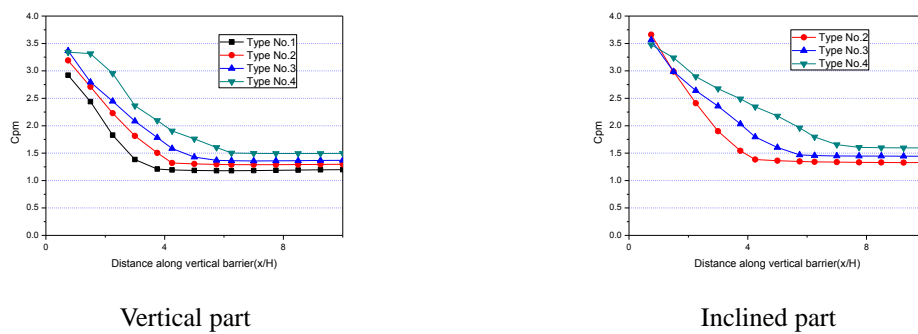


Fig. 15 Envelope of the mean nett pressure coefficients for NMS

Table 3 Average mean nett pressure coefficients for the inclined part of NMS at-grade

Zone	Configuration No.1	Configuration No.2	Configuration No.3	Configuration No.4
A(0<X<2H)	-	3.32	3.28	3.35
B(2H<X<4H)	-	1.95	2.34	2.69
C(X>4H)	-	1.34	1.51	1.81

### 5. Conclusions

Numerical simulation research on four typical configurations of NMS was carried out. In order to improve the numerical accuracy, a careful consideration of all important aspects, for example, the turbulence model as well as the model parameters, the boundary conditions and the mesh discretization etc., was made. Additionally, the numerical validation of one configuration with the wind tunnel test data was made.

Through systematic analyses of the wind load characteristics with the inclined part and the wind incidence angle, it was found that the addition of an inclined part to a noise mitigation structure at-grade affects the mean nett pressure coefficients on the vertical part, and that the extent of this effect depends on the length of the inclined part itself. The magnitudes of the mean

nett pressure coefficients for both the vertical part and the inclined part of NMS at-grade tend to increase with length of inclined part.

Finally, a comparison with the wind load code British/European Standard BS EN 1991-1-4:2005 was made and the envelope of the mean nett pressure coefficients of the noise mitigation structures was given for design purposes.

The research for this paper was mainly conducted by means of a numerical simulation method; nevertheless, some unavoidable numerical errors would affect the numerical accuracies, which are limited by the turbulence model, the difference scheme, the mesh discretization etc.

The research described should be helpful in improving current wind codes, by suggesting more reasonable wind pressure coefficients for different configurations of noise mitigation structures, and finally, the wind-resistant safety of the NMS structural design will be improved.

## Acknowledgements

The study reported in this paper is carried out under the support of the RGC General Research Fund, HKSAR Project No. 9041338. Financial supports from the National Natural Science Foundation of China under Grant Nos. 50708014 and 51178441, and the Fundamental Research Funds for the Central Universities are also gratefully appreciated.

## References

- Baker, C.J. (2001), "Unsteady wind loading on a wall", *Wind Struct.*, **4**(5), 413-440.
- Barić, E., Džijan, I. and Kozmar, H., (2010), "Numerical simulation of wind characteristics in the wake of a rectangular building submitted to realistic boundary layer conditions", *Transact. Famena*, **34**(3), 1-10.
- British/European Standard BS/EN 1991-1-4:2005 (2005), *Eurocode 1: Actions on structures-Part 1-4: General actions – Wind actions*.
- Buildings Department, Hong Kong (2004), *Code of practice on wind effects in Hong Kong*, Government of the Hong Kong Special Administrative Region, Buildings Department, Mongkok, Hong Kong, China.
- Blocken, B., Stathopoulos, T. and Carmeliet, J. (2007), "CFD simulation of the atmospheric boundary layer: wall function problems", *Atmos. Environ.*, **41**(2), 238-252.
- Durbin, P.A. and Petterson Reif, B.A. (2001), *Statistical theory and modeling for turbulent flows*, John Wiley & Sons Press, Chichester.
- Engineering Sciences Data Unit (1989), *Boundary walls, fences and hoarding: mean and peak wind loads and overturning moments*, ESDU Data Item 89050, (revised 1990).
- Franke, J., Hellsten, A., Schlünzen, H. and Carissimo, B. (2007), "Best practice guideline for the CFD simulation of flows in the urban environment", COST Office, Brussels, ISBN 3-00-018312-4. <http://www.mi.uni-hamburg.de/Official-Documents.5849.0.html>.
- Gorlé, C., van Beeck, J. and Rambaud, P. (2010), "Dispersion in the wake of a rectangular building: validation of two reynolds-averaged navier-stokes modelling approaches", *Bound-Lay. Meteorol.*, **137**(1), 115-133.
- Guerts, C. and van Bentum, C. (2010), "Wind loads on T-shaped and inclined free-standing walls", *Wind Struct.*, **13**(1), 83-94.
- Holmes, J.D. (2001). "Wind loading of parallel free-standing walls on bridges, cliffs, embankments and ridges", *J. Wind Eng. Ind. Aerod.*, **89**, 1397-1407.
- Kozmar, H. (2011), "Wind-tunnel simulations of the suburban ABL and comparison with international standards", *Wind Struct.*, **14** (1), 15-34.

- Labovský, J. and Jelemenský, L. (2011), "Verification of CFD pollution dispersion modelling based on experimental data", *J. Loss Prevent. Proc.*, **24**(2), 166-177.
- Letchford, C.W. (2001), "Wind loads on rectangular signboards and hoardings", *J. Wind Eng. Ind. Aerod.*, **89**(2), 135-151.
- Letchford, C.W. and Holmes, J.D. (1994), "Wind loads on free-standing walls in turbulent boundary layers", *J. Wind Eng. Ind. Aerod.*, **51**, 1-27.
- Letchford, C.W. and Robertson, A.P. (1999), "Mean wind loading at the leading ends of free standing walls", *J. Wind Eng. Ind. Aerod.*, **79**(1-2), 123-134.
- Menter, F.R. (1994), "Two-equation eddy-viscosity turbulence models for engineering applications", *AIAA J.*, **32**(8), 1598-1605.
- O'Sullivan, J.P., Archer, R.A. and Flay, R.G.J. (2011), "Consistent boundary conditions for flows within the atmospheric boundary layer", *J. Wind Eng. Ind. Aerod.*, **99**(1), 65-77.
- Parente A., Gorié C., van Beeck, J. and Benocci, C. (2011), "A comprehensive modelling approach for the neutral atmospheric boundary layer: consistent inflow conditions, wall function and turbulence model", *Bound. – Lay. Meteorol.*, **140**(3), 411-428.
- Richards, P.J. and Quinn, A.D. (2002), "A 6 m cube in an atmosphere boundary layer flow, Part 2. Computational solutions", *Wind Struct.*, **5**(2-3), 177-192.
- Shum, K.M., Hitchcock, P.A., Wong, K.S. et al. (2011), "Wind loading on noise mitigation structures in Hong Kong", *Proceedings of the 13th International Conference on Wind Engineering ICWE13*, Amsterdam, July.
- Wang, D.L., Zheng, L. and Chen, A.R. (2011), "Running cars induced wind loads on sound barrier of elevated roads", *Adv. Mater. Res.*, **378-379**, 137-142.
- Yang, W., Quan, Y., Jin, X.Y., Tamura, Y. and Gu, M. (2008), "Influences of equilibrium atmosphere boundary layer and turbulence parameter on wind loads of low-rise building", *J. Wind Eng. Ind. Aerod.*, **96**(10-11), 2080-2092.
- Yang, Y., Gu, M., Chen, S.Q. and Jin, X.Y. (2009), "New inflow boundary conditions for modeling the neutral equilibrium atmospheric boundary layers in Computational Wind Engineering", *J. Wind Eng. Ind. Aerod.*, **97**(2), 88-95.
- Yang, Y. and Gu, M. (2012), "New inflow boundary conditions for modelling the neutral equilibrium atmospheric boundary layer for the SST  $k-\omega$  model", submitted to *J. Wind Eng. Ind. Aerod.*
- Zheng, S. and Wang, L.M. (2009), "Study on the wind load shape coefficients of railway noise barriers", *China railway sci.*, **30**(4), 46-50. (Chinese)